Chaos
An Interdisciplinary Journal of Nonlinear Science

RESEARCH ARTICLE | MAY 28 2024

Fractal structures in the chaotic advection of passive scalars in leaky planar hydrodynamical flows FREE

Special Collection: Topics in Nonlinear Science: Dedicated to David K. Campbell's 80th Birthday

Ricardo L. Viana ; Amanda C. Mathias ; Leonardo C. Souza ; Pedro Haerter

Check for updates

Chaos 34, 053136 (2024)
https://doi.org/10.1063/5.0197988

View Online
Export Citation

29 May 2024 12:24:52

AIP Publishing



Chaos ARTICLE pubs.aip.org/aip/cha

Fractal structures in the chaotic advection of passive scalars in leaky planar hydrodynamical flows

Cite as: Chaos 34, 053136 (2024); doi: 10.1063/5.0197988
Submitted: 15 January 2024 · Accepted: 6 May 2024 ·
Published Online: 28 May 2024

View Online Export Citation CrossMark

Ricardo L. Viana,[a] Amanda C. Mathias, Leonardo C. Souza, and Pedro Haerter

AFFILIATIONS

Departamento de Física, Universidade Federal do Paraná, Curitiba, PR 81531-990, Brazil

Note: This paper is part of the Focus Issue on Topics in Nonlinear Science: Dedicated to David K. Campbell's 80th Birthday.
[a]**Author to whom correspondence should be addressed:** viana@fisica.ufpr.br

ABSTRACT

The advection of passive scalars in time-independent two-dimensional incompressible fluid flows is an integrable Hamiltonian system. It becomes non-integrable if the corresponding stream function depends explicitly on time, allowing the possibility of chaotic advection of particles. We consider for a specific model (double gyre flow), a given number of exits through which advected particles can leak, without disturbing the flow itself. We investigate fractal escape basins in this problem and characterize fractality by computing the uncertainty exponent and basin entropy. Furthermore, we observe the presence of basin boundaries with points exhibiting the Wada property, i.e., boundary points that separate three or more escape basins.

Published under an exclusive license by AIP Publishing. https://doi.org/10.1063/5.0197988

29 May 2024 12:24:52

Chaotic advection of particles in two-dimensional hydrodynamical flows has various applications in many fields, from meteorology and oceanography to chemical engineering. One of the outstanding properties of chaotic trajectories of advected particles is large-scale transport and mixing. In some situations, time-dependent hydrodynamical flows can be translated to non-integrable open Hamiltonian systems. The underlying dynamics of chaotic advections in leaky two-dimensional flows leads to a number of fractal structures that can be characterized using suitable diagnostics. In the case of two escape basins, we used an entropy-like quantity to quantify the final-state uncertainty and observed that the latter increases with the perturbation strength. For three or more escape basins, the corresponding basin structure is considerably more involved, presenting interior points, boundary points, and Wada points. These are points belonging to boundaries common to all basins and indicate an extreme form of fractality.

I. INTRODUCTION

Advection is the transport of a substance or quantity by the flow of a fluid, i.e., the properties of the substance are transported by the flow.[1] There are several engineering applications of advection, like the transport of pollutants, sedimentation, mixtures, and emulsions.[2,3] In the biological context, the advection of blood particles can cause the formation of atherosclerotic plaques.[4] Other applications of advection can be found in meteorology and oceanography, from the transport of quantities like heat, moisture, salinity, etc., due to atmospheric and oceanic flows, respectively.[5–8] Active processes in chemical and biological systems are also strongly affected by chaotic advection.[9,10]

A simplification in the modeling of these phenomena considers the advection of passive scalars in such a way that they are transported by the flow but without interacting with the flow itself.[1] In this approximation, the speed of the advected particles is equal to the fluid velocity at each point. If, moreover, we suppose an incompressible two-dimensional flow, the equations of motion are formally identical with Hamilton's equations.[9,11] This fact enables us to use the powerful machinery of Hamiltonian dynamics to investigate advected particle motion. In particular, if the fluid flow presents an explicit time-dependence, the resulting Hamiltonian system is non-integrable and its phase space turns out to be neither entirely regular nor entirely chaotic.[12] The regular part consists of periodic and quasiperiodic orbits, while chaotic orbits fill densely a finite region of the phase space.[13]

Published under an exclusive license by AIP Publishing

Chaotic advection has been extensively investigated in the literature, since the seminal work of Aref,[14] where it was introduced a blinking vortex model describing stirring. Other models have been proposed over the years for this purpose.[1] Actually chaotic transport is thought to lead to efficient mixing in time-dependent two-dimensional fluid flows. One question that arises in this investigation is how to quantify the mixing of two or more substances caused by chaotic advection.[15]

In this work, we propose an approach to tackle chaotic advection problems by considering the fractal structures appearing in chaotic orbits of non-integrable Hamiltonians representing leaky planar hydrodynamic flows.[16] The systems must have leaks in order to allow the inflow of different substances that mix together. Our treatment, however, is limited to the dynamical aspects of this mixing.[17] Microscopic effects related to particle diffusion and chemical reactions are thus neglected, although they can play an important role when small spatial scales are involved.[18] Moreover, the particles are supposed not to interact with the flow, an assumption that may not be true when finite-size effects are considered.[19,20] Chaotic advection has been studied in open hydrodynamical flows, like the flow in the wake of a cylinder, where the phenomenon has been connected with chaotic scattering.[21,22] In the present paper, however, we shall consider a flow confined by fixed barriers, with leaks through which particles can escape.

The fractal structures we are dealing with in this work are escape basins, which are sets of initial conditions leading to escaping orbits after a sufficiently long time. The fractal character of the escape basin boundaries can be measured by some quantifiers, originally developed for attractors in dissipative dynamical systems.[16] The uncertainty exponent, for example, has been devised to quantify the final-state uncertainty of initial conditions related to the presence of fractal basin boundaries. In a Hamiltonian system, we can adapt this concept to fractal escape basin boundaries and use it to estimate the box-counting dimension of the common frontier.[23] This method has been already applied for a model of the von Kármán vortex street of a viscous fluid around a cylinder,[10] a blinking vortex-sink system,[24] and an alternating sinusoidal shear flow model.[17] In the latter work, Altmann *et al.* have shown how to mix the system for a certain perturbation value, quantifying the fractality and uncertainty related to basin boundaries. It has been pointed out that the fractal structures in leaky planar flows are responsible for the typical filamentation observed in chaotic flows.[25]

Another measure used to this purpose is the so-called basin entropy, which considers the probability of a given initial condition escaping through some exit in phase space.[26] The basin entropy provides an alternative way to estimate the escape basin boundary dimension.[27] We have previously used such quantifiers to investigate fractal structures in the escape basin structures in various open Hamiltonian systems, like the drift motion of charged particles in magnetized plasmas,[28] magnetic field lines in Tokamaks,[29,30] light scattering by a system of two rotating black holes,[31] etc. In the present paper, we will consider a model of time-dependent two-dimensional flow in which exits are suitably positioned in order to reveal the corresponding fractal escape basin structure. The uncertainty exponent and the basin entropy are thus used to quantify final-state uncertainty related to the fractal structures present in the flow. In the case of three or more basins, we verified and quantified the so-called Wada property, which is a non-trivial topological feature by which boundary points have neighborhoods with points of all basins, irrespective of their sizes.[32]

The rest of this article is organized as follows: in Sec. II, we outline the model of two-dimensional flow with explicit time-dependence to be used here. Section III discusses escape basins and their underlying mathematical structure. Section IV deals with the quantitative characterization of fractal structures using the uncertainty exponents and basin entropies. The Wada property and its quantitative characterization are discussed in Sec. V. Section VI is devoted to our conclusions.

II. DOUBLE GYRE FLOW

Ideal fluid flows (without viscosity and heat conduction) can be described by five scalar fields:[33] pressure $p(\mathbf{r},t)$, density $\rho(\mathbf{r},t)$, and velocity $\mathbf{v}(\mathbf{r},t)$. These scalar fields are determined by solving balance equations obtained from conservation principles of mass, linear momentum, and energy, provided suitable boundary conditions are defined. Mass conservation, when applied to incompressible flows for which density is space and time-independent, leads to the condition $\nabla\cdot\mathbf{v}=0$.

Considering two-dimensional flows restricted to a plane $z=0$, the incompressibility condition reads

$$\frac{\partial v_x}{\partial x}+\frac{\partial v_y}{\partial y}=0, \tag{1}$$

which is identically satisfied if we define a stream function $\psi(x,y,t)$ such that the velocity Cartesian components are $v_x=-\partial\psi/\partial y$ and $v_y=\partial\psi/\partial x$. Using these relation, it follows that $d\psi=v_y\,dx-v_x\,dy=0$, in such a way that streamlines represent a family of curves for which $\psi=const$.

Passive advection is the transport of a scalar by the fluid flow such that the presence of the transported scalar does not alter the flow. Hence, the velocity of the advected particles is the same as the flow velocity, and the equations of motion for them are

$$\frac{dx}{dt}=-\frac{\partial\psi}{\partial y}, \tag{2}$$

$$\frac{dy}{dt}=\frac{\partial\psi}{\partial x}, \tag{3}$$

which can be identified as Hamilton's equations, where y is the generalized coordinate, x is the corresponding canonically conjugated momentum, and the Hamiltonian turns out to be the stream function $H=\psi$. If the latter does not depend on time, the Hamiltonian is an integral of motion. In this case, since there is only one degree of freedom, the Hamiltonian system is integrable.

As a consequence of integrability, we can find a canonical transformation from (x,y) to action-angle variables (J,ϑ), in such a way that the new Hamiltonian depends only on the action variable $\psi(x(J,\vartheta),y(J,\vartheta))=H(J)$.[12] The equations of motion then read

$$\frac{dJ}{dt}=-\frac{\partial H}{\partial\vartheta}=0, \tag{4}$$

29 May 2024 12:24:52

Published under an exclusive license by AIP Publishing

$$\frac{d\vartheta}{dt} = \frac{\partial H}{\partial J} \equiv \omega(J), \tag{5}$$

where ω is the corresponding frequency.

Starting from initial conditions (J_0, ϑ_0), the above system of equations is solved as

$$J(t) = J_0 = \text{const.}, \tag{6}$$

$$\vartheta(t) = \omega(J_0)\, t + \vartheta_0, \tag{7}$$

such that phase trajectories are straight lines in the $J - \vartheta$ plane, the motion along them being periodic with period ω. The Hamiltonian is said to satisfy the so-called *twist condition* if ω has no extrema, i.e.,

$$\frac{\partial \omega}{\partial J} \neq 0. \tag{8}$$

Otherwise, the system is *non-twist*, for which ω does not vary monotonically with J, and the dynamical properties can be considerably different from a twist system.[5]

Now, consider that the situation where the stream function depends explicitly on time $\psi = \psi(x, y, t)$. The system is no longer integrable since the Hamiltonian is not an integral of motion. In this work, we are concerned with models of planar vortices with finite extension, limited by stagnation curves. One example is the following stream function:[34,35]

$$\psi(x, y) = \psi_0 \sin(\pi x) \sin(\pi y), \tag{9}$$

where ψ_0 is a positive constant. This model, however, is not a proper solution of the hydrodynamical equations, but rather a simplified version of multiple-vortex structures that often occur in flows of geophysical interest.[6]

We limit the phase space to the rectangle $\mathcal{R} = \{0 \leq x \leq 2, 0 \leq y \leq 1\}$ in order to describe a minimal model consisting of just two vortices (double gyre). The equilibrium points, in this case, are (Fig. 1)

$$\begin{aligned} &Q_1 : (1/2, 1/2)\,, \quad Q_2 : (3/2, 1/2)\,, \\ &S_1 : (0, 1), \quad S_2 : (1, 1), \quad S_3 : (2, 1), \\ &S_4 : (0, 0), \quad S_5 : (1, 0), \quad S_6 : (2, 0). \end{aligned}$$

A linear stability analysis shows that Q_1 and Q_2 are centers, hence marginally stable. Numerical integration of Eqs. (2) and (3) confirms that they are also nonlinearly stable since the trajectories in their neighborhoods are closed curves encircling them (Fig. 1). The six equilibria S_i are saddle points mutually connected by heteroclinic trajectories formed by straight line segments, which act as frontiers of the two vortices centered at Q_1 and Q_2, with clockwise and counterclockwise rotations, respectively. There are four horizontal heteroclinic connections $H_{1,2,3,4}$ and three vertical ones $V_{1,2,3}$. In particular, the vertical segment V_2 separates the two vortices contained in the rectangle $\mathcal{R}$ (Fig. 1).

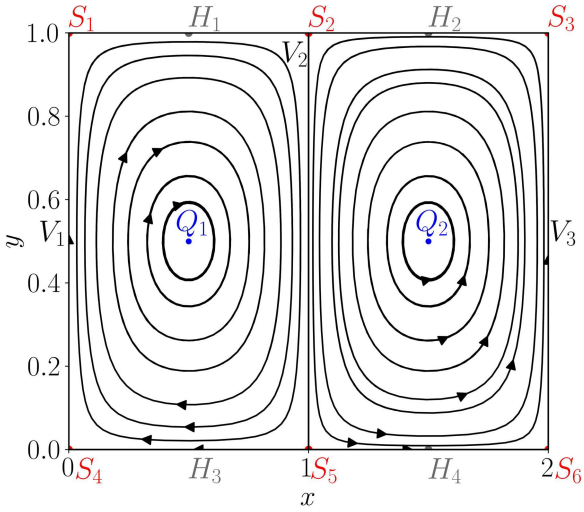


FIG. 1. Trajectories of advected particles for the time-independent double gyre flow with stream function given by (9), with $\psi_0 = 0.1$.

The explicit time-dependence can be included in the following way:[34]

$$\psi(x, y, t) = \psi_0 \sin[\pi f(x, t)] \sin(\pi y), \tag{10}$$

where the time-dependent term is periodic with frequency Ω and reads

$$f(x, t) = a(t)\, x^2 + b(t)\, x, \tag{11}$$

$$a(t) = \delta \sin(\Omega t), \tag{12}$$

$$b(t) = 1 - 2\delta \sin(\Omega t), \tag{13}$$

where δ is a "small" parameter, which stands for the strength of non-integrability of the system. Indeed, as $\delta \to 0$, we have $a = 0$ and $b = 1$ such that the system reduces to the integrable case.

Hamilton's equations referring to the stream function (10) are

$$\frac{dx}{dt} = -\pi\, \psi_0 \sin[\pi f(x, t)] \cos(\pi y), \tag{14}$$

$$\frac{dy}{dt} = \pi\, \psi_0 \cos[\pi f(x, t)] \sin(\pi y) \left(\frac{\partial f}{\partial x}\right). \tag{15}$$

Notice that, even if $\delta \neq 0$, there remain some invariant lines. For example, at $y = 0$ and $y = 1$, we have $\dot{y} = 0$, and thus, the heteroclinic trajectories $H_{1,2,3,4}$ are preserved. Moreover, since

$$f(x = 2, t) = 4a + 2b = 4\delta \sin(\Omega t) + 2 - 4\delta \sin(\Omega t) = 2,$$

it follows that $\sin[f(2, t)\pi] = \sin(2\pi) = 0$ and $\dot{x} = 0$. Consequently, the heteroclinic trajectories $V_{1,3}$ are also preserved by the perturbation, and the perturbed fluid flow as a whole remains confined to the rectangle $\mathcal{R}$ for all times. However, the vertical line V_2 is not preserved for $\delta \neq 0$, and thus, the flow of the two vortices becomes able to reach most points of $\mathcal{R}$.[35]

29 May 2024 12:24:52

Published under an exclusive license by AIP Publishing

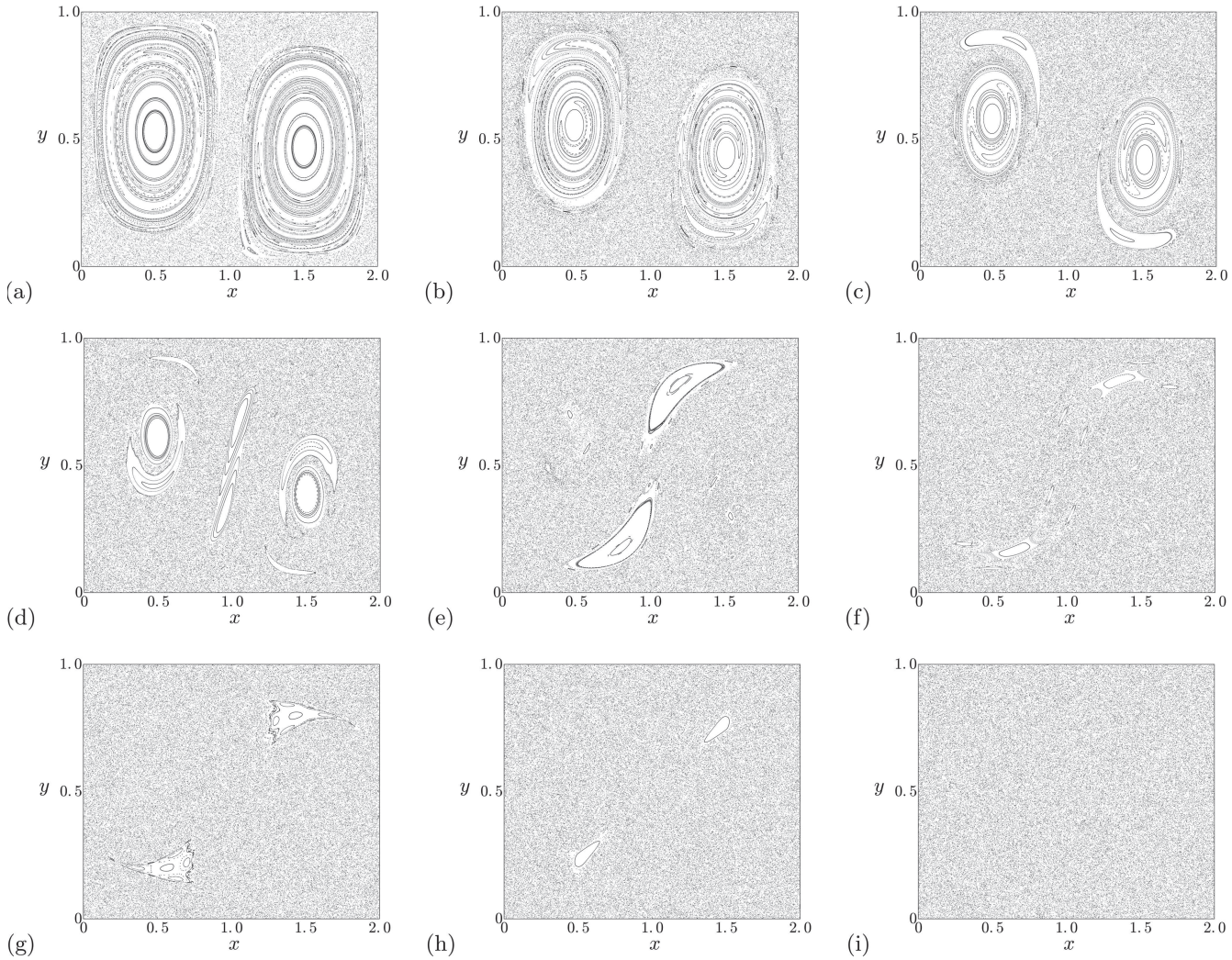


FIG. 2. Phase portraits of the time-T map for the time-dependent double gyre flow (10), when $\psi_0 = 0.25$, $T = 1.0$, and $\delta =$ (a) 0.15, (b) 0.25, (c) 0.35, (d) 0.45, (e) 0.55, (f) 0.65, (g) 0.75, (h) 0.85, (i) 0.95.

We solve numerically Eqs. (14) and (15) for given values of the parameters ψ_0, δ, and Ω, as well as suitably chosen initial conditions (x_0, y_0). Since the system is periodic, we can sample phase space variables at integer multiples of the perturbation period $T = 2\pi/\Omega$, by defining the following discrete variables:

$$x_n = x(t = nT), \quad y_n = y(t = nT), \tag{16}$$

such that we obtain a stroboscopic (time-T) map

$$\begin{pmatrix} x_{n+1} \\ y_{n+1}, \end{pmatrix} = \mathbf{F} \begin{pmatrix} x_n \\ y_n, \end{pmatrix}, \tag{17}$$

which is invertible, i.e., there is a unique inverse map $\mathbf{F}^{-1}$, as well as area-preserving ($|\det \mathbf{DF}| = 1$) since the map is derived from numerical integration of Hamilton's equations.

Figure 2 shows phase portraits corresponding to some orbits of this stroboscopic time-T map $\mathbf{F}$ when $\psi_0 = 0.25$ and $T = 1.0$, for different values of δ. The rectangle $\mathcal{R}$ remains invariant, whereas the vertical segment V_2 no longer exists, hence there will be a flow from one cell to another, corresponding to the chaotic orbit related to the heteroclinic tangle arising whenever $\delta \neq 0$. For small δ, a number of quasiperiodic tori within each vortex is preserved, in accordance with the Kolmogorov-Arnold-Moser (KAM) theorem, as well as periodic islands related to resonances [Fig. 2(a)].[13]

An increase of the perturbation strength [Figs. 2(b)–2(d)] causes the enlargement of the chaotic area-filling orbit through the destruction of invariant curves and part of the vortices are engulfed into the larger chaotic sea. As the parameter δ increases, however, other phenomena also take place as the emergence of stable periodic islands at regions formerly occupied by the chaotic sea [Figs. 2(e)

29 May 2024 12:24:52

Published under an exclusive license by AIP Publishing

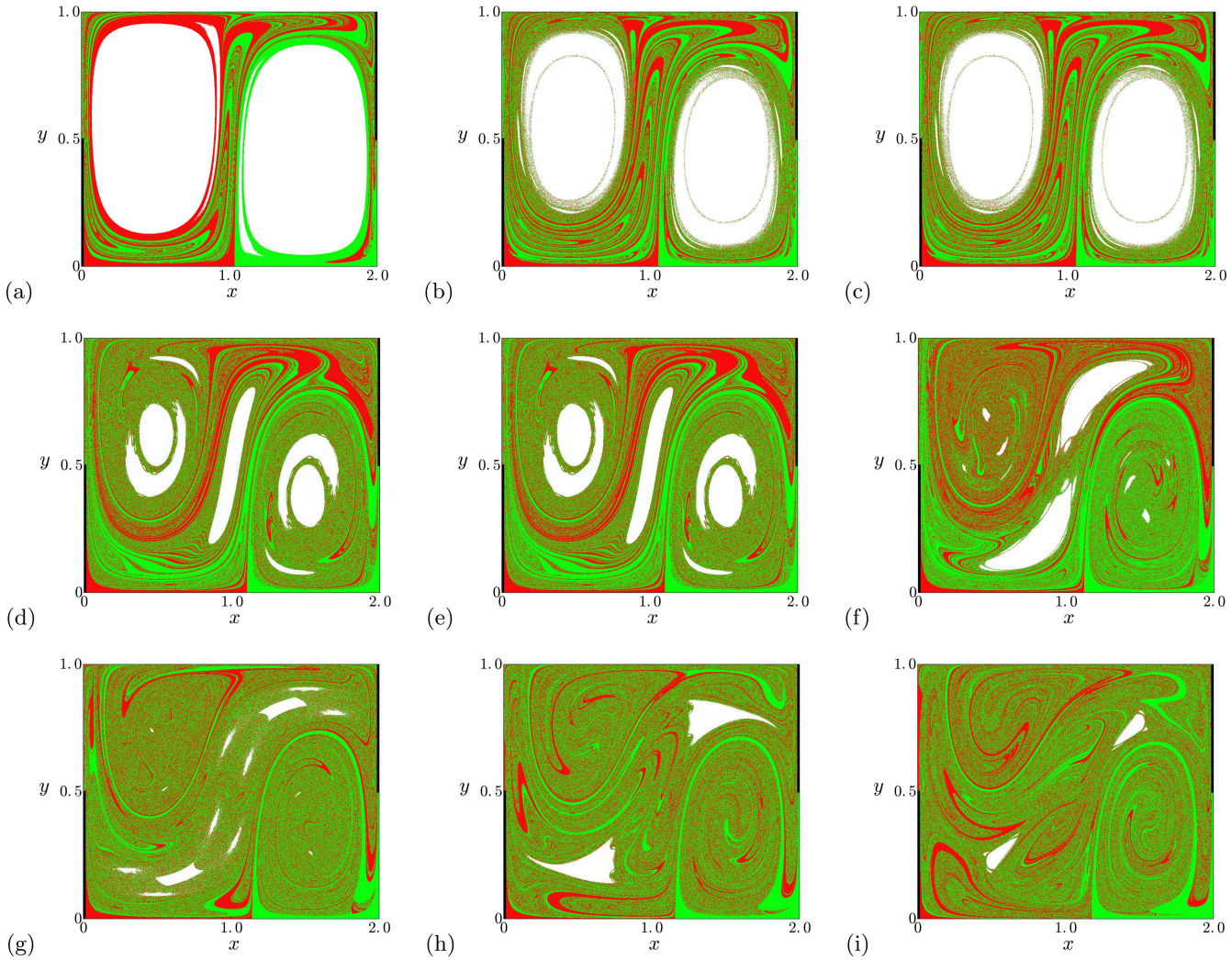


FIG. 3. Escape basins corresponding to the exits A (red pixels) and B (green pixels) of the time-T map for the double gyre flow (10), when $\psi_0 = 0.25$, $T = 1.0$, and $\delta =$ (a) 0.15, (b) 0.25, (c) 0.35, (d) 0.45, (e) 0.55, (f) 0.65, (g) 0.75, (h) 0.85, (i) 0.95. The exits are depicted by the thick black vertical lines placed at the left and right boundaries.

and 2(f)], whereas the previous vortices have disappeared. This process, for δ large enough, results in an almost completely chaotic flow [Figs. 2(g)–2(i)]. There still remains, though, a tiny portion of the phase space occupied by islands too small to be seen unless a further magnification is used.

III. ESCAPE BASINS

Since the rectangle $\mathcal{R}$ is kept invariant under the time-dependent flow, it makes a closed Hamiltonian system. In order to turn it into an open Hamiltonian system, we introduce one or more exits (or leaks) that can be chosen either as holes carved on the rectangle walls or collector plates placed inside $\mathcal{R}$. The set of initial conditions in $\mathcal{R}$ leading to trajectories escaping through a given exit is called its corresponding escape basin $\mathcal{B}$.[36] The escaping advected particles leak from the system without modifying the flux itself. In other words, the flow does not escape a given region but rather the advected particles that do not return after escaping (this has been called a "resetting mechanism"), see Ref. 37.

Initially, we will consider two exits, placed at the following positions near the boundary of $\mathcal{R}$:

$$\mathrm{A}: (0.00 \le x \le 0.01, 0.0 \le y \le 0.5), \tag{18}$$

$$\mathrm{B}: (1.99 \le x \le 2.00, 0.5 \le y \le 1.0). \tag{19}$$

Let us consider a particle placed at the initial condition (x_0, y_0). If, after a sufficiently large number of iterations of the stroboscopic map, the current particle position (x_n, y_n) escapes from the rectangle

29 May 2024 12:24:52

Published under an exclusive license by AIP Publishing

$\mathcal{R}$ through the exit A (respectively, B), we say that (x_0, y_0) belongs to the escape basin of that exit, denoted as $\mathcal{B}$(A) [respectively, $\mathcal{B}$(B)].

We have performed the following numerical experiment. We covered the rectangle $\mathcal{R}$ with a fine mesh of points, each of them tested as an initial condition (x_0, y_0) for the stroboscopic time-T map. The corresponding orbit is followed until, after a large enough number of map iterations, we have the following outcomes: the orbit either escapes through exits (i) A, (ii) B, or (iii) it does not escape at all. Since the exits were positioned at regions where the motion is chiefly chaotic, the non-escaping trajectories are likely to be placed on tori undestructed by the time-dependent perturbation.

In Fig. 3, we depict the basins of escape for exits A and B, for different values of perturbation strength δ. Points belonging to the basin $\mathcal{B}$(A) are painted red, whereas points of $\mathcal{B}$(B) basin are depicted in green. The white regions indicate initial conditions that do not escape within a pre-specified large time of 10^4 map iterations (we have varied this time by some orders of magnitude without seeing noticeable changes). This is the case, for example, of the closed orbits characterizing the vortices at each side of the rectangle since the corresponding particles do not escape at all [Figs. 3(a)–3(c)].

As the perturbation strength δ further increases, other changes occur like the formation of a new periodic island between the two original vortices [Fig. 3(d)]. The center of this island undergoes a saddle-center bifurcation, becoming a saddle point and generating two new centers [Fig. 3(e)]. Other such changes are observed until the island becomes too small to be distinguished (within the resolution used) [Figs. 3(f)–3(i)].

The convoluted nature of the escape basins revealed by Fig. 3 is actually a consequence of the dynamics underlying the chaotic regions containing area-filling orbits that surround the periodic islands, eventually occupying most of the phase space. The key ingredient here is the heteroclinic tangle of invariant manifolds of unstable periodic orbits embedded in the chaotic sea. Such manifolds extend virtually over all the chaotic region and eventually intercept the exits placed very near the rectangle $\mathcal{R}$, with a small width of $\sim$0.01.

It turns out that the boundary between the red and green escape basins is the stable manifold of a chaotic saddle in this region. In order to understand this fact, let us consider the action of the map $\mathbf{F}$ and its inverse $\mathbf{F}^{-1}$ on sets of points in the two-dimensional phase space. The stable and unstable invariant manifolds emanating from an unstable periodic orbit P of the map $\mathbf{F}$ are denoted by $W^s(P)$ and $W^u(P)$, respectively.

According to Fig. 4, we consider a segment Σ of the escape basin boundary intercepting the unstable manifold of an unstable periodic orbit P, embedded in a chaotic orbit. The backward images of the segment Σ, like $\mathbf{F}^{-1}(\Sigma)$ and $\mathbf{F}^{-2}(\Sigma)$, are smoothly deformed, becoming increasingly narrow along the direction of $W^u(P)$ and elongated along $W^s(P)$. In other words, as the number of map iterations goes to infinity, the escape basin boundary converges to the stable manifold of P.

This happens because the intersections between the unstable manifold and the basin boundary converge exponentially fast according to the corresponding eigenvalue of the tangent map $\mathbf{DF}(P)$. The length of the lobes formed by the backward images increases to preserve areas. Hence, if the boundary segment Σ crosses the unstable (or stable) manifold of the chaotic saddle, the escape basin boundary is fractal.[10]

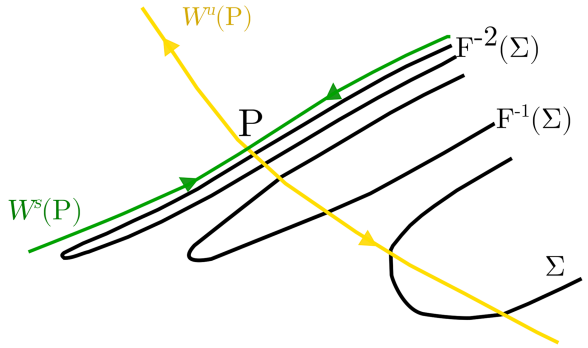


FIG. 4. Schematic figure showing the accumulation of the escape basin filaments toward the stable manifold (red) of an unstable periodic orbit embedded in a chaotic region.

IV. CHARACTERIZATION OF FRACTAL ESCAPE BASINS

In any dynamical system, one of the paramount questions is how to predict the future outcome of the trajectories, given the initial conditions. For open Hamiltonian systems, where the trajectories can exit a certain phase space region through two or more exits, the predictability refers to what exit will a given initial condition evolve to, as the time is long enough. In order to answer that question, it is important to analyze the geometry of the escape basin boundary, using the uncertainty exponent technique.[9]

Let us consider the boundary Σ between two escape basins, say, $\mathcal{B}$(A) and $\mathcal{B}$(B). Any initial condition placed in the rectangle $\mathcal{R}$ is determined within a given uncertainty ϵ. In the two-dimensional phase space, this is represented by a small disk of radius ϵ centered at the initial condition. If the entire disk is contained in either $\mathcal{B}$(A) or $\mathcal{B}$(B), the corresponding initial condition evolves to a well-defined exit with certainty. If, on the other hand, this disk intercepts the escape basin boundary Σ, the initial condition is ϵ-uncertain. The fraction of ϵ-uncertain condition scales as ϵ^α, where $\alpha = 2 - d$ is the uncertainty exponent and d is the dimension of the boundary Σ.[38]

If the latter is a smooth curve ($d = 1$), it turns out that $\alpha = 1$, i.e., the fraction of uncertain conditions scales linearly with ϵ: we may think of a narrow strip of width $\sim \epsilon$ at both sides of Σ and only the disks intercepting that strip would lead to uncertain initial conditions.[23] However, if the escape basin boundary is fractal, then $1 < d < 2$, leading to an exponent $0 < \alpha < 1$. This fact imposes serious difficulties to long-term prediction of to what exit will a given initial condition evolve to. Even a huge effort spent at diminishing the uncertainty ϵ will lead to a modest decrease in the uncertain fraction. This problem worsens as $\epsilon \to 0$ since in this limit, practically no improvement in the initial condition determination will have any effect on final-state prediction.

Final-state uncertainty caused by fractal basin boundaries can be also be characterized by the so-called basin entropy.[26] The basic idea is to divide the rectangle $\mathcal{R}$ into a fine mesh of N boxes, each of

29 May 2024 12:24:52

Published under an exclusive license by AIP Publishing

which containing a number of sample initial conditions. If we have N_A possible exits we define a map which associates to each initial condition a single variable (called a color) labeled from 1 to N_A. The color in each grid point represents the value of an integer random variable j. Denoting p_{ij} the probability that the jth color is assigned to the ith box, the basin entropy of the ith box is defined as

$$S_i = -\sum_{j=1}^{N_A} p_{ij} \log p_{ij}, \quad (i = 1, 2, \ldots, N), \tag{20}$$

in such a way that the total basin entropy is obtained summing up all N boxes in the mesh

$$S_b = \frac{1}{N} \sum_{i=1}^{N} S_i. \tag{21}$$

If we had considered just one exit ($N_A = 1$), then $p_{ij} = 1$ for all i and j, hence $S_b = 0$, i.e., there would be no uncertainty in the final state. On the other hand, if we have had N_A exits, each of them with the same probability $p = 1/N_A$, then S_b would take on its maximum value $\log N_A$. In this case, the uncertainty would also be maximal. Another quantity of interest is the entropy of the escape basin boundary S_{bb}, which is defined in the same way as before, but considering only those boxes containing more that one color, which cover the boundary Σ.

In the first place, we consider two exits, just like in Sec. II, where we obtained numerical approximations for their corresponding escape basins. The corresponding probabilities are normalized for each box i, hence $p_{i,1} + p_{i,2} = 1$, and the basin entropy reads

$$S_b = \frac{1}{N} \sum_{i=1}^{N} \left\{ p_{i,1} \ln p_{i,1} + p_{i,2} \ln p_{i,2} \right\}. \tag{22}$$

Each box with side length ϵ contains N_p^2 pixels such that, for the ith box, the corresponding probability $p_{i,1}$ takes on a discrete value out of the following set:

$$p_{i,1} \in \left[0, \frac{1}{N_p^2}, \frac{2}{N_p^2}, \ldots, 1 - \frac{1}{N_p^2}, 1 \right]. \tag{23}$$

Those boxes for which either $p_{i,1} = 0$ or 1 do not contribute to the computation because the entropy is zero in such cases. The other values of $p_{i,1}$ are the contributions of the boxes at the escape basin boundary, for they contain pixels belonging to both basins. Thus, the possible values of $p_{i,1}$ for the remaining N_b boxes are given by $p_m = m/N_p^2$, where $m = 1, 2, \ldots, N_p^2 - 1$. Let us denote by q_m the fraction of the N_b boxes, and S_m is the entropy of the mth box. The basin entropy can be expressed as[39]

$$S_b = -\frac{N_b}{N} \sum_{m=1}^{N_p^2} q_m S_m = -C \frac{N_b}{N}, \tag{24}$$

where C is a constant which depends on the fraction q_m. For fractal basin boundaries, the values of q_m are known to obey a Gaussian-like distribution.[39]

From its definition, the basin entropy is closely related to the box-counting dimensions of an escape basin and its corresponding boundary, denoted by d and D, respectively. If there are necessary N boxes with (suitably normalized) side length ϵ to cover the rectangle $\mathcal{R}$, it turns out that $N \sim \epsilon^{-d}$. By the same token, if N_b boxes are needed to cover the basin boundary then $N_b \sim \epsilon^{-D}$. Substituting on (24), we obtain that the basin entropy scales with ϵ^{d-D}, where $d - D$ is an uncertainty exponent.[26] It is defined in a slightly different way as before, but their values are numerically so close that the difference is indistinguishable in practice.[39]

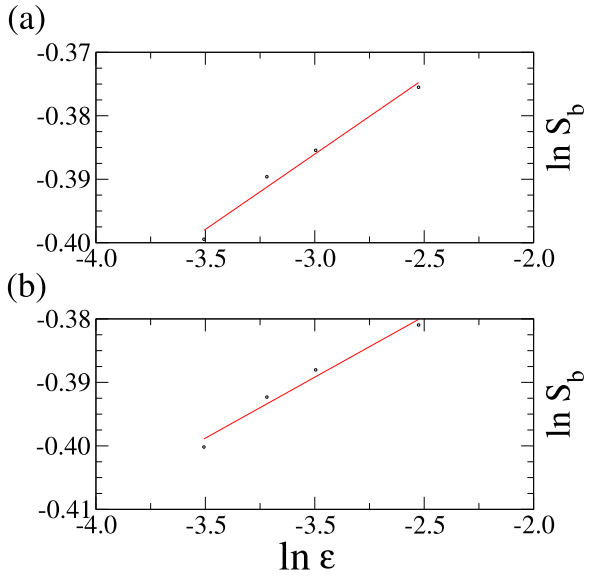


FIG. 5. Escape basin entropy as a function of box size for (a) $\delta = 0.75$; (b) $\delta = 0.85$.

We applied both quantifiers to the double gyre flow in the rectangle $\mathcal{R}$, with two exits given by (18) and (19). For each value of the box side length ϵ, we computed the basin entropy using (22), where we considered 10^5 iterations of the time-T map for a number of initial conditions therein such that those orbits that do not escape are removed from the statistics. The results are depicted in Fig. 5 for different values of ϵ. The least squares fits indicate, for two distinct perturbation strengths of $\delta = 0.75$ and 0.85, values of the escape basin boundary dimension equal to 1.976 and 1.981, respectively, which are very close to 2.0, indicating an area-filling escape basin boundary. These values are in accordance with a result of Lau *et al.*, which states that the dimension of the co-dimension of the fractal boundary for non-hyperbolic chaotic scattering (which is similar to our leaky flow chaotic advection) actually vanishes.[40]

The dimension of the escape basin boundary D is plotted in Fig. 6 as a function of the perturbation strength δ. For small values of the latter, the dimension grows rapidly from ~ 1.4 to ~ 1.8. For intermediate and higher values of the perturbation δ, the dimension increases to values close to 2.0, including the two examples mentioned in the previous paragraph. As a trend, the final-state uncertainty for the determination of the exit through which the orbit escapes increases with the perturbation, reaching the limit of area-filling curves expected for strongly non-hyperbolic system.

29 May 2024 12:24:52

Published under an exclusive license by AIP Publishing

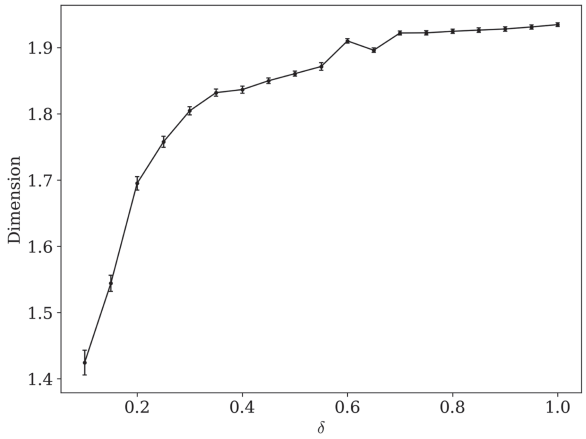


FIG. 6. Dimension of the escape basin boundary as a function of the perturbation strength δ.

We show in Fig. 7 our results for the basin and boundary entropies, as well as the relative area of the red escape basin, as a function of the perturbation parameter δ. As a general trend, both entropies increase with δ, indicating that the escape basins become progressively more intertwined with increasing perturbation. For relatively large perturbation δ, the basin entropy seems to saturate at a value near ~ 0.60, which is close to the theoretical limit of $\ln 2 \approx 0.69$. Hence, the basins may become highly intertwined, but the corresponding exits are not exactly equiprobable.

For all considered values of δ, the basin boundary entropy S_{bb} (black triangles) is higher than the basin entropy S_b (blue squares). This is chiefly because less boxes are required to cover the basin boundary than the basins themselves. On the other hand, the difference between S_b and S_{bb} decreases with δ, and the basin boundary entropy has a smaller variation interval between 0.60 and 0.65.

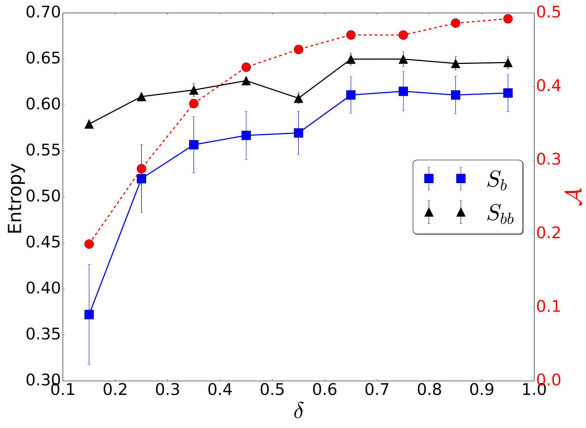


FIG. 7. Escape basin entropy (blue), basin boundary entropy (black), and relative area $\mathcal{A}$ of the red escape basin $\mathcal{B}(R)$ (red) as a function of the perturbation strength δ.

A possible reason for the overall increase of entropy with δ is the similar behavior displayed by the relative area $\mathcal{A}$ of red basin, depicted in Fig. 7 using red circles. As δ is large enough, this fraction approaches 0.5, suggesting a nearly equiprobable scenario.

V. CASE OF THREE ESCAPE BASINS

Given that two escape basins typically have a fractal boundary, with measurable consequences in terms of final-state predictability, one may well ask what would be the corresponding situations for three or more escape basins. If a point has a neighborhood consisting just of points belonging to a single escape basin, it is called an interior point. A boundary point P for the basin $\mathcal{B}$ is such that every open neighborhood of P intersects both the basin $\mathcal{B}$ and at least another basin $\mathcal{B}' \neq \mathcal{B}$.

If P is a boundary point of at least three different basins, then P is called a Wada point. A boundary is said to has the Wada property if there are boundary points that are also Wada.[32,41] The Wada property can be regarded, in the present work, as an extreme form of fractality, leading to a loss of final-state predictability.[15]

The places where the exits are chosen have a small influence on the quantitative characterization of the escape basin structures, provided the exits are placed in regions with chaotic orbits and relatively few periodic islands. Accordingly we have chosen the following three exits:

$$\mathsf{C}: (0.10 \leq x \leq 0.15, 0.10 \leq y \leq 0.15), \tag{25}$$

$$\mathsf{D}: (1.85 \leq x \leq 1.90, 0.10 \leq y \leq 0.15), \tag{26}$$

$$\mathsf{E}: (0.10 \leq x \leq 0.15, 0.85 \leq y \leq 0.90). \tag{27}$$

We obtained the corresponding escape basin for these three exits using the same procedure already described for two exits. Our results are shown in Fig. 8(a), for a perturbation amplitude $\delta = 0.95$. Points belonging to the exit basins of C, D, and E are painted blue, red, and green, respectively. The basins are densely intertwined, as expected from their fractal nature, but a quantitative treatment is necessary to verify the Wada property. More specifically, what is the relative number of Wada points since there may be interior points (not belonging to any basin boundary) and points belonging to the boundary between just two attractors.

The so-called Nusse–Yorke criterion states that, in order that escape basins possess the Wada property, the unstable manifold of a periodic orbit intersects all the escape basins. This is a necessary but not sufficient condition to have the Wada property fulfilled.[42] Unfortunately, this criterion is difficult to apply in many systems. Moreover, this criterion does not inform about the fraction of Wada points.

Instead, we use the so-called grid approach:[43] we assume the existence of three exits in the rectangle R, which may be either carved in the boundary or be exhausting holes inside $\mathcal{R}$ (the treatment can be extended for an arbitrary number N_A of exits). We denote, by $\mathcal{B}_j, j = 1, 2, 3$, the corresponding basins of escape. The rectangle $\mathcal{R}$ is divided into a set of non-overlapping boxes $b_1, b_2, \ldots, b_k$. We iterate each point (x, y) of $\mathcal{R}$ so as to determine the corresponding escape basin $\mathcal{B}_j$.

29 May 2024 12:24:52

Published under an exclusive license by AIP Publishing

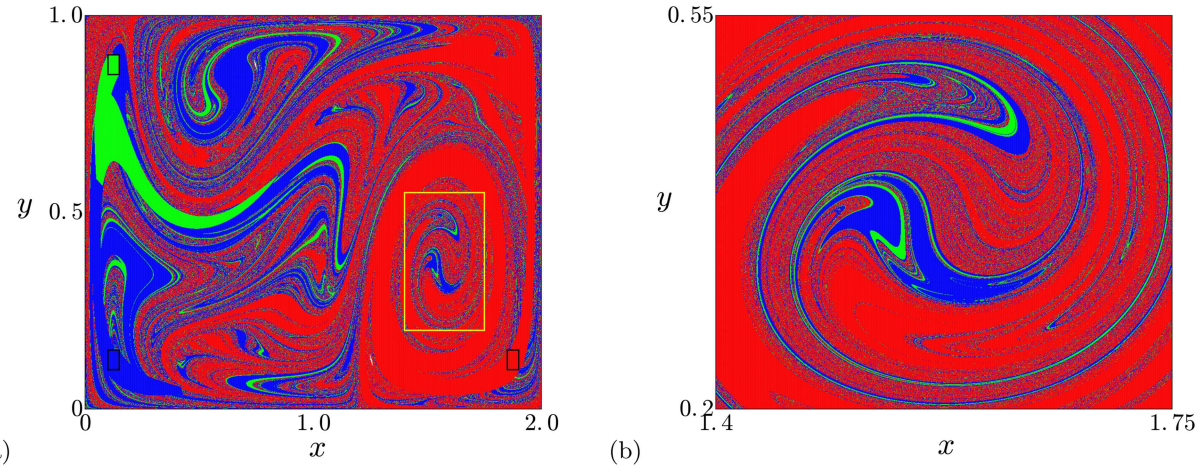


FIG. 8. (a) Basins of escape for the case of three exits. Points belonging to the basins of exits C, D, and E are painted blue, red, and green, respectively, for $\delta = 0.95$. (b) A magnification of a small region of (a).

Next, we defined $C(x, y) = j$ if $j \in \mathcal{B}_j$ and $C(x, y) = 0$ if (x, y) is in none of the sets, i.e., the value of C is the color of the box. For any rectangular box, we define $C(b) = C(x, y)$ where x, y is the point at the center of the box. We denote by $P(b_j)$ the collection of grid boxes formed by b_j and all boxes that have at least one point in common with b_j, in the two-dimensional case $P(b_j)$ is a 3×3 collections of boxes with b_j as the central box.

The number of different $C(b_j)$ (colors) in $P(b_j)$ for each b_j is $M(b_j)$. Provided $M(b_j) = 2$ for a given b_j, we take the two closest boxes in $P(b_j)$ with different colors and draw a line segment between them, determining the color of the midpoint of this line, that is, calculating to which basin it belongs. If the color of the segment midpoint is such that we have all the possible colors inside $P(b_j)$, then $M(b_j) = 3$ and we stop the procedure. Otherwise, we choose intermediate points in this line segment and repeat this procedure until $M(b_j) = 3$, unless, the number of points exceeds a specified limit.

The following sets are defined: (i) G_1 is a set containing points belonging to the interior of the jth escape basin (interior points); (ii) G_2 contains points belonging to the boundary between two escape basins, i.e., there are two different colors inside the set $C(b_j)$ (boundary points); (iii) G_3 consists of points that belong to the boundary between three basins, that is, the set G_3 contains points satisfying the Wada property (Wada points). After obtained the values of $M(b_j)$ for all grid points, we determine the set G_m of those original boxes such that $M(b_j) = m$, for a given integer m.

Let us denote by G_m^q the G_m set obtained at the qth refinement step. As q goes to infinity, the sequence of refinements is expected to converge to a stationary set G_m, and we compute the quantity

$$W_m = \lim_{q\to\infty} \frac{\mathcal{N}(G_m^q)}{\sum_{j=2}^{3} \mathcal{N}(G_j^q)} \quad (m = 2, 3), \tag{28}$$

where $\mathcal{N}(G_j^q)$ is the number of points of the set G_j at the qth refinement step. If $W_m = 0$, the system has no grid boxes belonging to the boundary separating m escape basins, whereas if $W_m = 1$, all the boxes belong to the common boundary of m escape basins. The system is said to have full Wada property if $W_3 = 1$, for it will be always possible to find any color arbitrarily close to the boundary between two other colors. The system is said to be partially Wada when $0 < W_m < 1$, with $m \geq 3$.

In the case of $N_A = 3$ escape basins, we computed W_2 and W_3 after a number large enough of refinement steps. The relative contribution of each set is obtained by counting the respective fraction of points,

$$W_2 = \frac{\mathcal{N}(G_2)}{\mathcal{N}(G_2) + \mathcal{N}(G_3)}, \tag{29}$$

$$W_3 = \frac{\mathcal{N}(G_3)}{\mathcal{N}(G_2) + \mathcal{N}(G_3)}. \tag{30}$$

It is an important check to verify, for each qth refinement step, whether or not points of G_2 may belong to G_3: we test a number of initial conditions which are intermediate between the central box and a neighbor box with different color. If some of these initial conditions exhibit the missing color, then the central box is reclassified as G_3.

Figure 9(a) shows the distribution of the sets G_m for the escape basin structure depicted in Fig. 8. We plot the points classified as G_1, G_2, and G_3 using black, red, and blue pixels, respectively. It is quite evident a predominance of Wada points over boundary and interior points. The sheer existence of the latter indicates that the Wada property is only partially fulfilled, in this case.

In order to quantify the Wada property, we plot in Fig. 9(b), the values W_2 and W_3 as a function of the refinement step q. After $q = 10$ refinement steps, we have a convergence to the values $W_2 \approx 0.09$ and $W_3 \approx 0.91$, since $W_2 + W_3 = 1$. Hence, the Wada property is partially verified but more than 90% of the points are Wada, indicating a strong presence of this non-trivial property.

29 May 2024 12:24:52

Published under an exclusive license by AIP Publishing

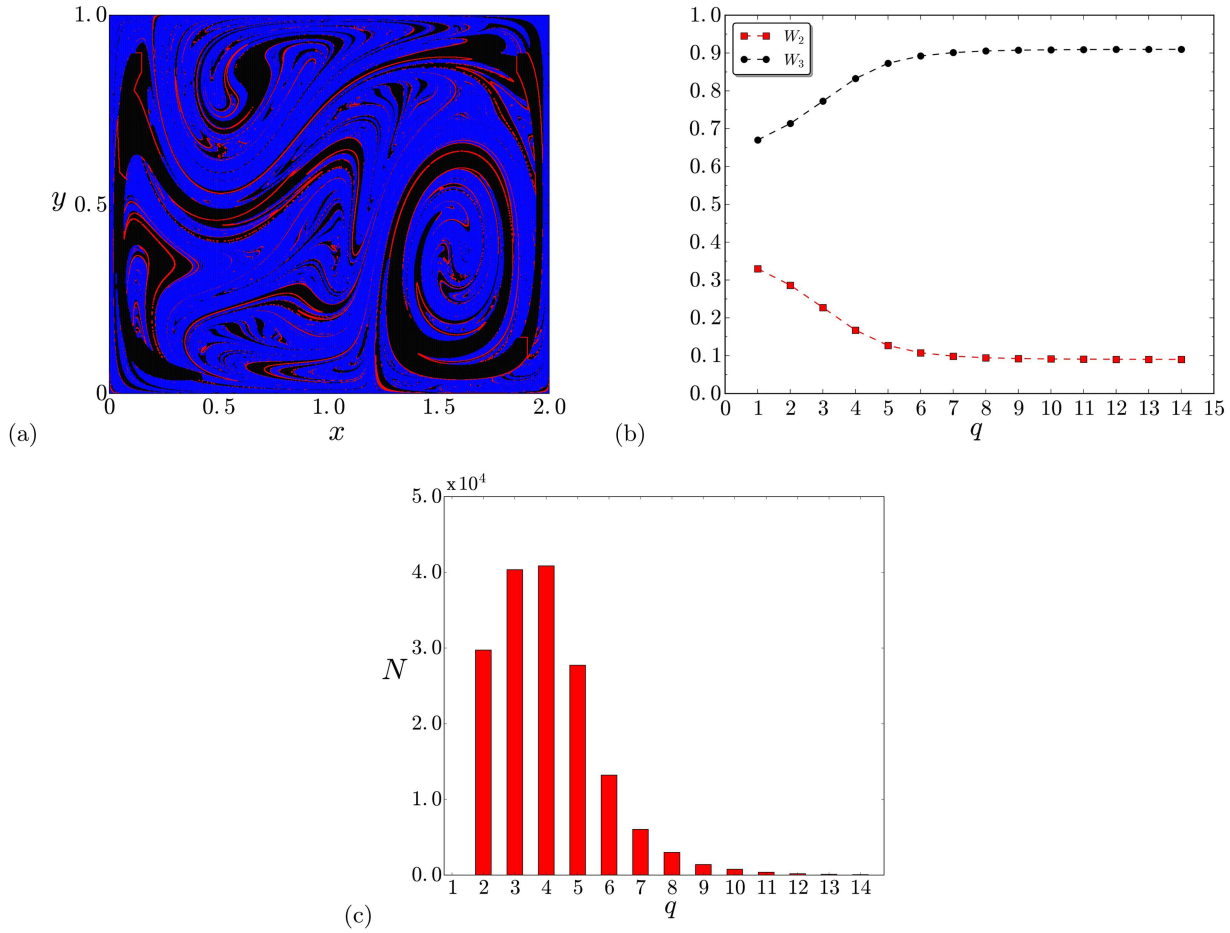


FIG. 9. (a) Basin structure of Fig. 8(a), showing points belonging to G_1 (interior points, black), G_2 (boundary points, red), and G_3 (Wada points, blue), after $q = 14$ refinement steps. (b) Values of W_2 (red) and W_3 (black) as a function of the refinement step. (c) Distribution of the number of reclassified points with the number of refinement steps.

Figure 9(c) depicts a distribution for the number of points initially classified as belonging to the set G_2 but which are reclassified to the G_3 set at each refinement step, after a large number of evaluations of the quantities W_2 and W_3. The convergence is already good enough after 3 to 5 refinement steps, and the number of reclassified points actually vanishes as $q \to \infty$.

VI. CONCLUSIONS

The two-dimensional incompressible flow of an ideal fluid is a Hamiltonian dynamical system with one degree of freedom. If a time-dependent perturbation is included, the system becomes nonintegrable and the dynamics can be described by standard results of Hamiltonian theory. One of them is the existence of an infinite number of heteroclinic points characteristic of area-filling chaotic orbits. In hyperbolic chaotic systems, the dynamics underlying the heteroclinic tangle is equivalent to the Smale horseshoe, which has a chaotic invariant set (a chaotic saddle).[44] In conservative systems, there are a number of fractal structures related to this set, such as escape basins in open conservative systems.

In this paper, we investigated the fractality of escape basins in an open two-dimensional flow (double gyre) with a time-dependent perturbation. In the case of two escape basins, we determine the uncertainty dimension of the corresponding fractal boundary and found it to be close to 2, which is the dimension of the underlying phase space. Such strongly fractal curves present almost insurmountable difficulties with respect to final-state prediction, i.e., it is utterly impossible to determine to what exit will a given trajectory escape through, given a small but nonzero uncertainty ϵ in the initial condition position.

The number of ϵ-uncertain initial conditions is known to scale with the boundary dimension d as $f(\epsilon) \sim \epsilon^{2-d}$. If we improve the accuracy with which the initial condition is known by a factor of 2, then the fraction of uncertain points is $f(\epsilon/2) \sim 2^{d-2} f(\epsilon)$. For a typically strong perturbation intensity, we found, using the concept of basin entropy, that the dimension of the escape boundary is

29 May 2024 12:24:52

Published under an exclusive license by AIP Publishing

$d \approx 1.981$, i.e., the uncertain fraction is $f(\epsilon') = 0.987 f(\epsilon)$, an improvement of just 1.3 %: a deceptive small outcome for such a big effort in improving initial condition accuracy.

Given this strikingly non-trivial behavior for basins of two escapes, we expect similar difficulties for three or more basins. In fact, such cases lead to the so-called Wada property: if we draw a circle of radius ϵ centered at some point with such property, there will be pieces of all the basins within the circle, no matter how small ϵ may be. In general, there can be three kinds of points: interior points (which do not belong to any boundary), boundary points (involving two basins only), and Wada points. For a given value of the perturbation strength, we determined that ca. 91% of the points have Wada property, in such a way that the latter is partially fulfilled.

We choose the double gyre model because it is relatively simple to analyze since the model equations keep the system boundaries invariant. In general, however, the boundaries themselves can change with time-dependent perturbations, and in such cases, the determination of exits and the corresponding basins is more difficult. However, the general characteristics of the strong fractality exhibited by the escape basins are expected to be present in more realistic examples of time-dependent planar hydrodynamical incompressible flows. These can be used to model, for example, pollutant escape from flows of oceanographic or meteorological interest.[45,46]

ACKNOWLEDGMENTS

This work was completed thanks to the financial support from São Paulo Research Foundation (FAPESP, Brazil) under Grant No. 2023/16146-6, and the Brazilian Federal Agency CNPq under Grant Nos. 403120/2021-7, 301019/2019-3, and 140920/2022-6.

AUTHOR DECLARATIONS

Conflict of Interest

The authors have no conflicts to disclose.

Author Contributions

Ricardo L. Viana: Conceptualization (lead); Formal analysis (lead); Funding acquisition (lead); Investigation (equal); Project administration (lead); Resources (equal); Writing – original draft (lead); Writing – review & editing (equal). **Amanda C. Mathias:** Data curation (equal); Formal analysis (equal); Investigation (equal); Methodology (equal); Software (equal); Supervision (equal); Visualization (equal); Writing – review & editing (equal). **Leonardo C. Souza:** Data curation (equal); Formal analysis (equal); Investigation (equal); Methodology (equal); Resources (equal); Software (equal); Validation (equal); Visualization (equal); Writing – review & editing (equal). **Pedro Haerter:** Data curation (equal); Investigation (equal); Methodology (equal); Resources (equal); Software (equal); Visualization (equal); Writing – review & editing (equal).

DATA AVAILABILITY

The data that support the findings of this study are available from the corresponding author upon reasonable request.

REFERENCES

[1] J. H. E. Cartwright, M. Feingold, and O. Piro, "An introduction to chaotic advection," in *Mixing: Chaos and Turbulence*, edited by H. Chaté *et al.* (Kluwer Academic, New York, 1999).
[2] J. M. Ottino, *The Kinematics of Mixing: Stretching, Chaos, and Transport* (Cambridge University Press, 1989).
[3] J. M. Ottino, Annu. Rev. Fluid Mech. **22**, 207 (1990).
[4] I. M. Silva, A. B. Schelin, R. L. Viana, and I. L. Caldas, Chaos **30**, 093135 (2020).
[5] D. del Castillo-Negrete and P. J. Morrison, Phys. Fluids A **5**, 948 (1993).
[6] C. Coulliette and S. Wiggins, Nonlinear Processes Geophys. **8**, 69–94 (2001).
[7] I. I. Rypina, M. G. Brown, F. J. Beron-Vera, H. Koçak, M. J. Olascoaga, and I. A. Udovydchenkov, J. Atmos. Sci. **64**, 3595 (2007).
[8] F. J. Beron-Vera, M. J. Olascoaga, M. G. Brown, H. Kocak, and I. I. Rypina, Chaos **20**, 017514 (2010).
[9] T. Tél, A. Moura, C. Grebogi, and G. Károlyi, Phys. Rep. **413**, 91 (2005).
[10] A. Pentek, Z. Toroczkai, T. Tel, C. Grebogi, and J. A. Yorke, Phys. Rev. E **51**, 4076 (1995).
[11] H. Aref, Annu. Rev. Fluid Mech. **15**, 345 (1983).
[12] A. J. Lichtenberg and M. A. Lieberman, *Regular and Chaotic Motion*, 2nd ed. (Springer Verlag, New York, 1992).
[13] E. Ott, *Chaos in Dynamical Systems*, 2nd ed. (Cambridge University Press, 2002).
[14] H. Aref, J. Fluid Mech. **143**, 1 (1984).
[15] Z. Toroczkai, G. Karolyi, A. Pentek, T. Tel, C. Grebogi, and J. A. Yorke, Phys. A **239**, 235 (1997).
[16] J. Aguirre, R. L. Viana, and M. A. F. Sanjuán, Rev. Mod. Phys. **81**, 333 (2009).
[17] E. G. Altmann, J. S. E. Portela, and T. Tél, Rev. Mod. Phys. **85**, 869 (2013).
[18] T. Tél, G. Károlyi, Á. Péntek, I. Scheuring, Z. Toroczkai, C. Grebogi, and J. Kadtke, Chaos **10**, 89 (2000).
[19] T. Nishikawa, Z. Toroczkai, C. Grebogi, and T. Tél, Phys. Rev. E **65**, 026216 (2002).
[20] R. D. Vilela, A. P. S. de Moura, and C. Grebogi, Phys. Rev. E **73**, 026302 (2006).
[21] C. Jung, T. Tél, and E. Ziemniak, Chaos **3**, 555 (1993).
[22] J. C. Sommerer, H.-C. Ku, and H. E. Gilreath, Phys. Rev. Lett. **77**, 5055 (1996).
[23] C. Grebogi, S. W. McDonald, E. Ott, and J. A. Yorke, Phys. Lett. A **99**, 415 (1983).
[24] G. Károlyi and T. Tél, Phys. Rep. **290**, 125 (1997).
[25] I. Tuval, J. Schneider, O. Piro, and T. Tél, Europhys. Lett. **65**, 633 (2004).
[26] A. Daza, A. Wagemakers, B. Georgeot, D. Guéry-Odelin, and M. A. F. Sanjuán, Sci. Rep. **6**, 31416 (2016).
[27] A. Daza, A. Wagemakers, and M. A. F. Sanjuán, Europhys. Lett. **141**, 43001 (2023).
[28] A. C. Mathias, R. L. Viana, T. Kroetz, and I. L. Caldas, Phys. A **469**, 681 (2017).
[29] J. S. E. Portela, I. L. Caldas, R. L. Viana, and M. A. F. Sanjuán, Int. J. Bifurcat. Chaos **17**, 4067 (2007).
[30] A. C. Mathias, T. Kroetz, I. L. Caldas, and R. L. Viana, Chaos, Solitons Fractals **104**, 588 (2017).
[31] E. E. de Souza Filho, A. C. Mathias, and R. L. Viana, Chaos, Solitons Fractals **150**, 111139 (2021).
[32] J. Kennedy and J. A. Yorke, Phys. D **51**, 213 (1991).
[33] L. D. Landau and E. M. Lifshitz, *Fluid Mechanics*, Course of Theoretical Physics Vol. 6 (Pergamon Press, Oxford, 1982).
[34] S. C. Shadden, F. Lekien, and J. E. Marsden, Phys. D **212**, 271 (2005).
[35] L. C. de Oliveira, C. G. L. Martins, M. Roberto, I. L. Caldas, and R. E. de Carvalho, Phys. A **391**, 6611 (2012).
[36] S. Bleher, C. Grebogi, E. Ott, and R. Brown, Phys. Rev. A **38**, 930 (1988).
[37] K. Ngan and R. T. Pierrehumbert, Phys. Fluids **12**, 822 (2000).
[38] S. W. McDonald, C. Grebogi, E. Ott, and J. A. Yorke, Phys. D **17**, 125 (1985).
[39] A. Gusso, R. L. Viana, A. C. Mathias, and I. L. Caldas, Chaos, Solitons Fractals **122**, 6 (2019).
[40] Y.-T. Lau, J. M. Finn, and E. Ott, Phys. Rev. Lett. **66**, 978 (1991).
[41] H. E. Nusse and J. A. Yorke, Phys. D **90**, 242 (1996).

29 May 2024 12:24:52

Published under an exclusive license by AIP Publishing

[42]L. Poon, J. Campos, E. Ott, and C. Grebogi, Int. J. Bifurcat. Chaos **6**, 251 (1996).
[43]A. Daza, A. Wagemakers, M. A. F. Sanjuán, and J. A. Yorke, Sci. Rep. **5**, 16579 (2015).
[44]Y.-C. Lai, C. Grebogi, J. A. Yorke, and I. Kan, Nonlinearity **6**, 779 (1993).
[45]K. V. Koshel and S. V. Prants, Phys.-Usp. **49**, 1151 (2006).
[46]S. Panchev, "Chaotic advection and geophysical applications (a review)," in *Air Pollution Modeling and Its Application XIII*, edited by S. E. Gryning and E. Batchvarova (Springer, Boston, MA, 2000).

29 May 2024 12:24:52

Published under an exclusive license by AIP Publishing